MEDWIN PUBLISHERS
Committed to create value for Researchers

Petroleum & Petrochemical Engineering Journal
ISSN: 2578-4846

Origin and Characterization of Joints in Sedimentary Rocks: A Review

Ghosh S[1]*, Milad B[1], Prasun S[2] and Ghosh SS[3]

[1]University of Oklahoma, Norman, Oklahoma, USA

[2]Louisiana State University, Baton Rouge, Louisiana, USA

[3]Kalinga Institute of Industrial Technology, Bhubaneswar, Odisha, India

Review Article

Volume 2 Issue 5

Received Date: July 28, 2018

Published Date: August 20, 2018

***Corresponding author:** Sayantan Ghosh, University of Oklahoma, Norman, Oklahoma, USA, Tel: +18016154307; Email: ghoshsayantan88@gmail.com

Abstract

Discontinuities are ubiquitous in all rocks at different scales. Their characterization occupies a high ground in the field of geological research. Discontinuity abundance, strength, flow and frictional properties are matters of great interest to structural geologists, petroleum engineers (mostly in unconventional shale gas and oil production), and civil engineers. Joints (opening mode fractures) are some of the most commonly observed rock discontinuities among others. Understanding joint origins from outcrops and other directly visible sources explain the presence of certain joints in the near and deep subsurface. We have summarized several tectonic and non-tectonic drivers behind joint origins and suggested the use of multiple supporting evidence while timing and causal interpretations are made. If particular subsurface joint sets may be traced back to the outcrops through the knowledge of their origins, their characteristics (length, aperture, height, abundance and interrelationships between these parameters) may be measured at the outcrops or using other data sources such as cores and image logs. Additionally, it is important to understand several non-visual data sources aiding in joint parameterization. This paper discusses the strengths and limitations of these direct (visual) and indirect (inference) data sources. In addition, we have summarized different methods for the quantification of the aforementioned joint related geometric and abundance parameters.

We have shown that each measurement method and data source has its own set of strengths and limitations, and the appropriate methods to be used are case specific. We suggest that, if possible, characterization by direct visualization (mainly outcrops) should not be withheld or substituted with techniques that only imply the presence of joints and faults. Also, reconciliation of all joint-related parameters (i.e., geometry and abundance) from all available data sources provide confidence in the geologic interpretation and models.

Keywords: Fractures; Rocks; Joint characterization; Microseismic; Seismic; Satellite; Velocity anisotropy; LIDAR

Introduction

A part of the geologic community is concerned about the mechanism of origin of natural fractures and the specific events that caused the fractures (i.e., origin timing). Engineers, on the other hand, concern themselves with natural fracture parameterization (size, shape, abundance) to understand their control and interaction with artificial hydraulic fractures in shales, stability of tunnels, mine pillars, and slopes. Although fracture timing is generally dealt with independently from fracture parameters such as orientation and size, they should not necessarily be treated as such. Understanding relative fracture timing may indicate fracture initiation mechanisms such as overpressure or folding. The knowledge of initiation mechanism may be indicative of the extent to which subsurface (invisible) fracture orientations may vary, and if their present orientation with respect to the prevailing stress field may enhance or impede engineering projects.

For instance, high density of 90° (vertical) to 45° dipping fractures may compromise the stability of mine support pillars. Similarly, for artificial hydraulic fracturing in a normal or strike-slip faulting stress regime, natural fractures oriented parallel to current SHmax (maximum horizontal stress) direction are likely to aid in long hydraulic fracture half lengths with large opening (Mode I) component. Natural fractures oriented perpendicular or at high angles to the SHmax, on the other hand, may result in complicated artificial hydraulic fracture patterns. In these cases, the knowledge of fracture timing and mechanism, implying fracture orientations, may aid such predictions.

Aydin [1] performed a commendable task of depicting discontinuities in shales using outcrops. He presented a synopsis of different structures found in sedimentary rocks and later mentioned the effect of these structures on artificial hydraulic fractures. He divided the end member failure behavior in shales, i.e., high strain fluid like (plastic or viscous deformation) behavior and low strain brittle behavior. In addition, the discontinuities were categorized into sharp (shear fractures [faults], joints, pressure solution seams) and diffuse (shear bands, compaction bands, dilation bands) categories. According to Aydin [1], sharp discontinuities are likely to occur in consolidated (relatively stiff) sediments, and diffuse discontinuities in poorly consolidated sediments aided by high overburden.

The bulk of our paper delves on quantifying joint (Mode I failure) parameters, and hereafter, joints will take precedence over other modes of failure. The terms “joint” and “fracture” have been used interchangeably to signify opening mode discontinuities with little to no shear displacement. We intend to present a summary of joint origins, existing methods of joint parameterization, and common data sources for deriving joint-related parameters. We have included a level of detail that is understandable to both geologist and engineers, i.e., the information on origin, methods, and data sources are not meant to be exhaustive.

Joint Origins

Origin-based joint classification falls into two main categories a) regional and b) tectonic. Regional joints have near constant orientations in widespread areas which results from a constant state of stress (either paleo or current). Tectonic joints are related to particular structure related to a local tectonic event. Tectonic joints may be further subdivided into "fault-related" and "fold-related" fractures. Fault-related joints may be shear fractures (oriented parallel or conjugate [60°] to the faults) or extensional fractures (bisecting the acute angle between faults). Splay joints are yet another type of tectonic joints formed due to a second episode of movement over preexisting joints or new faults. These joints usually form at an angle to the preexisting joints. However, to make such an inference for joints observed in the field, the sense of shear displacement on the preexisting joints should be consistent with the opening direction of the splay joints [2].

Fold related tectonic joints are oriented at specific angles to the fold axis and a pattern may be observed. Joints oriented parallel and perpendicular to the fold axis are interpreted as synfolding [3] and products of outer arc extension and layer parallel shortening respectively. Conjugate joints (or fractures with mm scale shear displacement) with an accompanied bisector perpendicular to the fold axis are also observed at several locations along the fold and interpreted as a product of layer parallel shortening. However, joints in kink folds with infinite curvature at the axial surface and zero curvature at the limbs are more difficult to predict. Bergbauer and Pollard [4] in their joint abundance model, reported an order of magnitude higher abundance in tectonic joint intensity compared to that of non-fold-related joints.

However, one should be careful while predicting the events leading to the origin of certain joint sets. Orientation relative to the fold is only one of the factors indicating joint origin. Information on orientation, in

addition to joint termination, crosscutting, cement fill, and knowledge of documented local and global tectonic events should be combined in a coherent manner to infer origin. Pollard and Aydin [2] suggest that joint sets that appear as conjugate sets (i.e., theoretical maximum horizontal stress probably bisected the acute angle) in the field should not be interpreted as such unless there is strong evidence for such interpretation. Regarding join branching, even though branches may be interpreted as having propagated at high velocities, there are cases where branching has taken place quasi-statically. Sometimes, two joints can join each other in an asymptotic manner leading to a fork-type appearance [2]. Additionally, the mechanism of joint arrest was attributed to a decrease in pore pressure and/or an increase in the remote stress perpendicular to the joint faces. The other arrest mechanism mentioned by the authors is interaction with obstacles such as other joints or local heterogeneities. These observations were derived from outcrop studies.

Regarding joint initiation, Pollard and Aydin [2] mentioned that tensile joints may originate even in a high compressive stress environment under high fluid pressure. Initiation of joints at flaws have been argued by introducing a stiffer and softer inclusion whose stiffness is much higher or lower respectively than the matrix. For elliptical shapes such as a crack, the remote compressive stress can be amplified many times in the form of local tension. Therefore, joints may initiate at some type of cavity. Grain contacts have also been mentioned as spots where cracks can initiate. Initiation may take place more easily with extra force from high pore pressure acting against the surrounding compressive forces. After joint initiation, the chemical reactions at the process zone near the tip may influence joint propagation [2]. The pore pressure also helps in joint propagation by increasing the driving stress which is the difference between the pore pressure and the remote compressive stress. With higher driving stresses, the stress intensity at the crack tip can exceed the fracture toughness of the material thus propagating the crack.

Cosgrove [5] mentioned that creation of natural hydraulic fractures is not restricted to early burial and diagenesis and can happen at any stage of basin evolution depending on the conditions. Episodic tensile fracturing, fracture propagation, and healing are possible during basin evolution. After the closing and healing, pressure can build up again (due to further burial) and reinitiate hydraulic fracturing. A buildup of fluid pressure in a sedimentary basin may result from disequilibrium compaction, increase in fluid temperature, kerogen cracking, diagenesis, and potentiometric head. Cosgrove [5] concluded that at any depth in the reservoir, the fracturing behavior can be different in two rock types. In order for shear failure to occur the Mohr's circle's diameter (i.e., the difference between maximum and minimum effective stress) must be more than four times the tensile strength of the rock at the time of failure. Otherwise, tensile failure will occur.

Lash and Engelder [6] observed numerous bed parallel microfractures in their study area. They mentioned that compaction disequilibrium (i.e., overpressure from the inability of fluid to escape) or bitumen cracking (i.e., oil generation) can locally increase the horizontal stress to values close to or greater than the vertical stress. Aided by low fracture toughness in the bedding direction, horizontal cracks can open against the vertical stress, even though the regional maximum stress direction may be vertical (i.e., normal faulting stress regime). However, in porous and silty (low clay) beds in their study area, bed parallel microcracks were not observed because the pores were likely large enough to be not completely filled, the permeability was higher causing fluid to drain locally, and lesser permeability and strength anisotropy prevailed due to circular (rather than flat) grains.

Ghosh, et al. [7] studied Woodford Shale fracture crosscutting/termination relationships and fracture cement under an optical microscope. Additionally, by unfolding (restoring) the beds, i.e., graphically returning the beds to their original flat positions (using stereonet), they found recurring joint sets that consistently strike in the same direction at different outcrop locations. Using these studies, they reported that the joint sets having consistent strikes (also containing bitumen at a few locations) were the oldest sets and of prefolding origin. The newer (non-bitumen filled) sets were fold related, and crosscut or abut the older bitumen-filled ones. They concluded that main joint sets that likely exist in the subsurface in the Woodford Shale are the two older sets that are of non-tectonic origin and may have initiated/propagated as a result of abnormally high pore pressure driven by bitumen cracking (i.e., hydrocarbon generation). Similarly, Pireh, et al. [8] reported the origin timing of five fracture sets in the Zagros Mountains. Two of the five sets were reported as not related to folding. Rest was related to different phases of rock folding and anticline formation.

In addition, to classification based on the origin timing, joints may be classified in terms of how they are bounded by the bedding planes. Some joints only traverse a single apparent bed and terminate at the bed boundaries at both

ends; they are classified as "perfect bed bounded". Others traverse several apparent beds but terminate at some type of bed boundary at both ends. These joints occurring in tandem with the perfect bed-bounded ones are classified as having a "hierarchical" pattern of bed boundedness [9]. Some vertical joints terminate abruptly at both ends without an apparent bed boundary. These are termed "unbounded". In another pattern, some taller joints terminate at mechanically significant interfaces with many shorter unbounded joints. Such an arrangement is termed "top bounded" [9]. However, no clear relationship exists between joint origin mechanisms and observed bed-boundedness patterns.

Joint Abundance Descriptions

Mauldon and Dershowitz [10] outlined several abundance definitions. In their classification, linear intensity (P10: number of fractures per unit length of scanline), areal intensity (P21: length of fracture traces per unit sampling area), volumetric intensity (P32: area of fractures per unit volume of rock mass) have units of "fractures/m". Linear porosity (P11: combined fracture apertures per unit length of scanline), areal porosity (P22: area of fractures per unit sampling area), and volumetric porosity (P33: volume of fractures per unit volume of rock mass) have units of fraction or "%" (or unitless). Areal density (P20: number of trace centers per unit sampling area) has a unit of "fractures/m^2"; volumetric density (P30: number of fracture centers per unit rock Volume) has a unit of "fractures/m^3." While P21, P20, P11, and P10 are possible to measure in the field or under a microscope, others are difficult to pin down.

There are three methods of obtaining the aforementioned abundance parameters. These are scanline sampling, window sampling, and circular window sampling methods [11]. In the scanline sampling method, fracture intensities (P10) are measured bed by bed along scanlines. In the circular window sampling method, the number of fracture intersections with a circle is divided by four times the circle radius to find the fracture intensity (P21) [11]. In the window sampling method, the total length of the fracture traces in an observed area (rectangular shape or other) is divided by the area to get the fracture intensity (P21) in fractures/m [12]. P10, P21, and P32 intensity values in any given area of observation do not always yield the same results. Mauldon and Dershowitz [10] provide conversion factors between the three parameters. However, P10, P21, and P32 should have identical values if measurements take place along scanlines oriented parallel to the normal of a fracture set [13].

Joint Data Sources

Joints may be characterized through direct observation or through indirect inference of fracture-related parameters. Figure 1 summarizes the data sources and the type of information that may be derived from such sources.

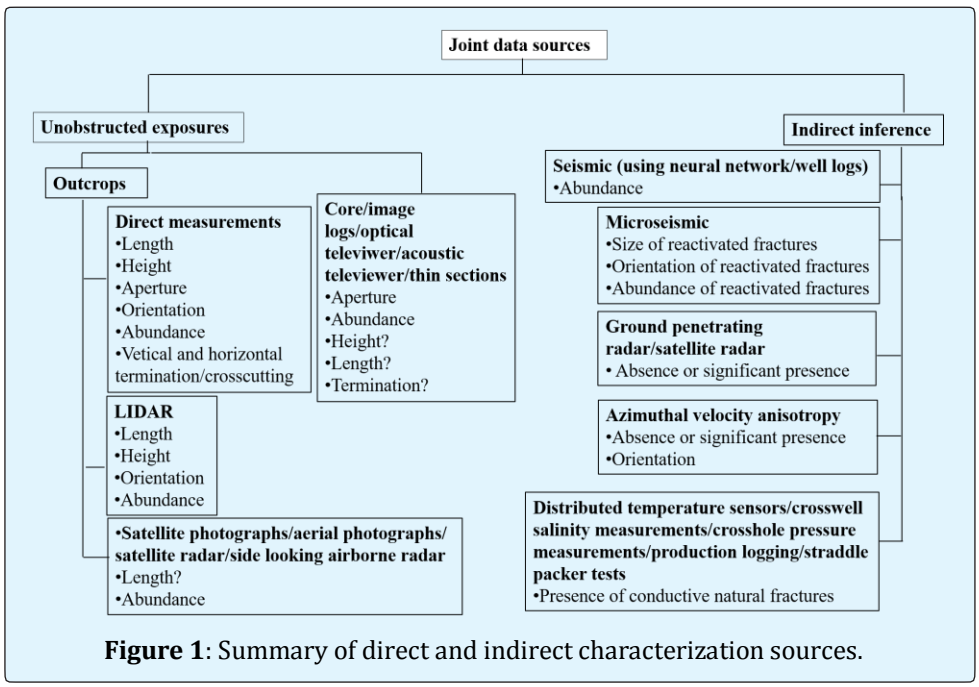

Figure 1: Summary of direct and indirect characterization sources.

Joint Characterization from Unobstructed Exposures

Outcrops

Direct Measurement: Zeeb, et al. [11] provide a detailed comparison of sampling methods from outcrops. They report that there is a lack of a general consensus on the minimum number of length (horizontal trace in map view) measurements required to adequately determine the length distribution of a fracture network. Additionally, correcting censoring bias can be challenging. Also, the minimum number of fractures need for the application of scanline sampling, window sampling, and circular window sampling need better constraint. Whether the lengths (i.e., in a map view) or heights (i.e., in a cliff-face view) are sampled along scanlines, there will be an underrepresentation of shorter fractures as they are less likely to be intersected [14].

Regarding joint length (horizontal trace in map view) measurements, being certain about the lengths is a requirement while performing length-aperture correlations. Whether a joint trace belongs to a single joint or multiple joints changes with the scale of view [11]. For example, a joint trace interpreted as single from far (such as satellite image) may turn out to be more than one distinct traces (i.e., linked or unlinked segments) when viewed up close. It may then be the onus of the interpreter to consider that as a single joint or more than one joint. Ghosh [15] defined relationships between joint length and height in the Woodford Shale using scanlines oriented perpendicular to joint length traces. He reported a suitable linear (length=5.65*height$^{0.85}$) or power-law (length=5.12*height+0.89) relationship between length (m) and height (m). Ghosh [12] showed correlations between joint length (m) and height (m) in the Hunton Group limestone with a linear (length=1.87*height+0.1095) or power law (length=2.06*height$^{0.85}$) best fit. Olson [16] reported a power-law relationship between fracture aperture and length. Ghosh [12] reported an average power law relationship (aperture=0.734*length$^{0.55}$) between joint aperture (mm) and length (m) in shales from multiple observations.

Ghosh [12] and Ghosh, et al. [7,17] counted joints along scanlines under an optical microscope to find microfracture intensity (fractures/m) and spacing in thin sections obtained from outcrops. Increasing joint intensity (P10) with decreasing bed thickness was observed. Additionally, Ghosh, et al. [17] showed a method of calculating P20 along an entire stratigraphic section of a shale formation using linear intensity (P10)-bed thickness relationships, and percentage of chert and shale beds in every stratigraphic foot (i.e., every 0.305 m) of the whole section. Hooker, et al. [9], on the other hand, used the scanline method to find P11 to measure strain (i.e., same as linear porosity) in outcrops and thin sections by plotting cumulative joint apertures along the length of the scanlines.

LIDAR: Light detection and ranging (LIDAR) is a method which substitutes direct measurement with laser derived images when sampling is required from a relatively large area. Images are obtained by illuminating a target (outcrop in this case) with laser light and measuring the time differential between the emission of the laser pulses and the reception of the reflected pulse. The return times of the each reflected pulse (assuming the speed of light as a constant) may be considered as individual points having cm to mm scale precision. Several of these points may be considered a point cloud. LIDAR works by grouping the point cloud into mesh triangles. The triangular elements are combined into groups based on the similarity of their dimensions and orientations. These groups may be fracture planes, bedding surfaces or other features. Using LIDAR, however, requires careful control of the spatial location, i.e., precise global positioning system location of the reflectors such as bedding planes and fractures. Best results are obtained when the scanner is oriented nearly perpendicular to the outcrop face. LIDAR also has filtering features that can remove the effect of vegetation thus generating enhanced rock images. Also, differential weathering (subtle differences in mineralogy) of rocks aid in improved LIDAR image interpretation. LIDAR generated fracture orientations, however, must be tallied with brunton measurements.

Hanzel [18] performed LIDAR based fracture characterization of the Woodford Shale. He used a LIDAR scanner (VZ-400) which can function in “long range mode” (pulse repetition rate: 100 kHz, effective measurement rate: 42000 measurements/s, measurement range: 280-600 m) and “high speed mode” (pulse repetition rate: 300 kHz, effective measurement rate: 122,000 measurements/s, measurement range: 160-350 m). In other words, obtaining a high-speed sampling requires decreased distance between the equipment and the outcrop. Accuracy and precision in both cases are 5 mm and 3 mm respectively. Hanzel [18] observed decreasing LIDAR intensity with increase in bed clay content, i.e., an inverse relationship between gamma ray (which increases with clay content) and LIDAR intensity

exists. Schlichtemeier [19] performed LIDAR measurements in a quarry exposing the Jackfork Group in Arkansas. The measurements were performed not only to quantify the fracture orientations but also to understand the lateral change in facies distribution of deepwater sediments. He reported an inverse logarithmic relationship between bed thickness and joint intensity in his study area. Portas [20] used LIDAR based measurements to quantify orientations, sizes, and roughness of several joint planes in a quarry exposing the Woodford Shale.

Satellite and Radar Imagery: Satellite imagery is another alternative when fracture characterization is required over a large area of interest. Ahmedhadi, et al. [21] made extensive use of aerial photographs and satellite imagery to map fractures termination patterns at different locations of an anticline. The termination information was used to identify fracture generation timing to interpret prefolding and synfolding fractures. Hilgers et al. [22], Holland, et al. [23,24] reported 650 lineaments with lengths ranging from 3-179 m using satellite images of Jabal Akhdar dome, Oman. Zeeb, et al. [25] used satellite images to evaluate the importance of fractures for the overall flow behavior in a fractured rock aquifer and to estimate the in-situ hydraulic apertures.

Dinger, et al. [26] mentioned water production trends from Eastern Kentucky. They reported productive water wells, i.e., ones that were at the 90th percentile in terms of water production to be located near fractured and faulted zones. Therefore, they delineated large fracture related lineaments in a 6,500 square mile area using side-looking airborne radar imagery (SLAR) and Landsat Thematic Mapper (TM) imagery (30-meter pixel resolution). Some of the wells later drilled in the delineated areas were above the 95th percentile of producing wells in the respective counties.

Image Logs and Cores: Image logs are obtained from pads that are in contact with the borehole wall and measure electrical resistivity. For image processing, high resistivity is generally set to brighter color and vice versa. Therefore, fractures containing hydrocarbons (high resistivity) may appear brighter compared to fractures containing brine (high conductivity). Additionally, resistivity images may be static (i.e., same color scheme for an entire well) or dynamic (running average type of color scheme to enhance resistivity contrast between features). Most resistivity imaging tools require conductive mud to operate. However, tools operating in non-conductive (i.e., oil based) mud are also available with their own limitations of fracture imaging.

In addition to resistivity image logs, two similar tools, i.e., optical televiewers and acoustic televiewers are available for borehole imaging. The optical televiewer uses a high-resolution digital camera and a light source providing real color and rock texture. It needs an empty borehole or a clear borehole fluid in order to work. The acoustic televiewer, on the other hand, uses a rotating sonar transducer and requires borehole fluid to be present in order to work [27]. Fractures appear as dark sinusoidal traces in the acoustic televiewer log since they reduce the amplitude of the reflected signal. Both optical and acoustic televiewers contain a magnetometer which orients the images with respect to the magnetic north. Images can be obtained as a wrapped image which resembles an external view of a core. Images can also be unwrapped (i.e., as if looking from the center of the borehole). Unoriented cores may be oriented using the images observed from the televiewers. The fracture information obtained from these logs contain dip direction, dip angle, and strike [27].

Constraining the spatial organization of vertical fractures in the subsurface is difficult using image logs from vertical wells as not many vertical fractures are captured. Image logs from horizontal wells help in this regard due to much higher intersections of vertical fractures with horizontal wells [28]. However, one should be careful regarding the fracture orientation while applying these methods. If the scanline is not oriented perpendicular to the fracture strike, the fracture intensity value will be underestimated (or spacing overestimated). A method for correcting orientation bias was suggested by Terzaghi [29], where the apparent spacing is multiplied by the cosine of the acute angle of the fracture normal and the scanline to obtain the true spacing [11]. However, this equation may result in the overestimation of the number of fractures (or underestimation of fracture spacing) that make low angle intersections, i.e., ones that are almost parallel to the wellbore.

Cores derived from the subsurface are another source of fracture abundance measurement. Since vertical cores only permit short scanlines (perpendicular to core length) for measurement of vertical fractures, Milad, et al. [30] used an area method of calculating fracture intensity in a Hunton Group Limestone core by dividing the total length of fractures by the slab/butt planar face area (i.e., P21 values) obtained every six inches (15.2 cm) of the core. Gale, et al. [31] on the other hand, used terms such as none, few, many etc. as descriptors of fracture abundance every 100 feet (30.5 m) of a vertical core. However, Gale's measurements should not be equated with horizontal scanlines measuring vertical fractures (even though the

resulting unit is in fractures/m), as the scanline (i.e., core length) is not oriented perpendicular to the fracture strikes. Gale, et al. [31] reported difficulty in quantifying serrated surfaces of the whole core and stated that planar core surfaces (i.e., core slab/butt faces) are more appropriate for quantifying fracture abundance. In addition, they took a shot at finding fracture surface area to core volume (P32) by observing the fracture trace heights and lengths and found values in the range of 0.33 to 4.01 fractures/m with a mean of 1.66 fractures/m in their studied core. Core fracture apertures in shales were found to range 30 μm-10 cm, with most in the range of 30 μm-1 mm. Fracture height measured in cores by Gale et al. core study ranges from < 1 cm to 1.8 m [31].

Joint Characterization from Indirect Indicators

While the aforementioned methods are direct ways to measure fracture parameters, several indirect methods also exist. Following sections briefly describe these methods.

Microseismic Imaging: Microseismicity, i.e., low magnitude earthquakes, occur during hydraulic fracturing jobs. These small earthquakes are recorded using downhole or surface receivers. It is commonly used in the oil and gas industry to understand the extent and geometry of the stimulated reservoir. Microseismic cloud patterns have been interpreted to emanate partly from natural fracture reactivation [32-34]. A method called seismic moment tensor inversion (SMTI) has been described by several researchers [35-38]. Using SMTI, the reactivated (failure) plane orientation, as well as the sense of movement (normal, thrust, opening, and closing) may be derived for the recorded microseisms.

Bosman et al. [39] used the SMTI not only to determine the natural fracture size and orientation at the treatment reservoir but also used the size and orientation information to understand natural fracture crosscutting, termination, connectivity, and effective reservoir permeability. According to Bosman, et al. [39] only natural fracture clusters that are connected to the well perforations (either directly or through the artificial hydraulic fracture) are effective in production. Isolated clusters not connected to the hydraulic fracture do not contribute to production.

Seismic Data (Utilizing Neural Networks and Well Logs): Seismic data is obtained by sending acoustic (sound) signals to the subsurface that are generated by surface-located sources and recording the reflected signals using surface receivers. Seismic imaging is useful at outlining discontinuities such as faults with substantial lateral displacement. However, fractures with minimal lateral displacement (or offset) such as joints are difficult to image. This imaging limitation can be overcome, however, using proxies for joint abundance. In that regard, a neural network may be used to estimate or model fracture abundance in the reservoir [40,41]. A neural network consists of information obtained from seismic data (fracture drivers) and information at the well location (fracture indicators). Fracture drivers may be classified as structure and geomechanics (bed slope, bed curvature, proximity to faults) related, seismic attribute (amplitude, elastic properties from prestack seismic inversion, acoustic impedance from poststack seismic inversion, azimuthal anisotropy, spectral imaging attributes) related [41]. Fracture indicators include fracture count from image logs and cores, fluid entry/exit locations from production logs, well-test permeability, shallow and deep resistivity differences, and drilling losses. In the neural network approach, the fracture drivers are ranked according to how reliably they are correlated to fracture indicators. Subsequently, the user chosen fracture drivers (geomechanical and seismic) are trained against the fracture indicators at the well. These relationships are then used to assign discrete fractures within the modeled reservoir [41].

Ground Penetrating Radar and Satellite Radar: Ground penetrating radar (GPR) assists in shallow subsurface imaging. The mechanism works by emitting pulses of high-frequency radio waves in the microwave band and detecting the reflected signals from subsurface structures. GPR acquisition and display methods are comparable to those of reflection seismic except that soil and shale at the surface impede GPR signal penetration. GPR frequencies used in stratigraphic studies range 10-100 MHz which provides 1.5-1 m vertical resolution [42-44]. This is substantially higher compared to the seismic resolution which is greater than 10-15 m. GPR is sensitive to rock electromagnetic properties, unlike reflection seismic that is sensitive to acoustic properties. Fine-grained materials, such as clay and silt, can hold more bonded water molecules compared to coarser-grained materials. High water content increases dielectric constant values. These finely grained lithologies under- or overlying coarsely grained lithologies result in high dielectric contrast and have greater visibility in GPR profiles [45].

The subsurface GPR images aid in the extension of outcrop observations into areas of poor or invisible rock exposures. A requirement for such extrapolations, however, is the knowledge of the formation lithologies and geometries from nearby outcrops or cores aiding in

the interpretation of GPR reflection boundaries. Pratt and Miall [46], Liner and Liner [47], and Beres, et al. [42] used low-frequency GPR in imaging large features such as major bounding surfaces and faults, but not detailed features such as joints or small-scale cross bedding. Martinez, et al. [45] on the other hand, used high-frequency GPR (500 MHz) with a penetrating depth of 3-4 m and was able to image fractures. In their study, joints exhibited diffraction, and when soil filled, showed slight velocity pull down.

Another GPR variation in which the source and the receivers are located in different wells, rather than on the surface, is also available. Jalali, et al. [48] used cross-hole GPR travel time tomography between injection boreholes. They mentioned that GPR velocity (i.e., electromagnetic wave velocity) depends on water content. Consequently, highly fractured zones that are water filled have low GPR velocity. According to Jalali, et al. [48], the low-velocity anomalies in their GPR velocity tomogram were strongly fractured zones. Though the GPR method mentioned by Jalali, et al. [48] was used in crystalline rocks, it may be used in sedimentary rocks as well to estimate relative fracture abundance.

In addition to seismic data and GPR, satellite radar can image the shallow subsurface. Laake [49] used satellite radar to scan 20 m below surface sand to map ancient river beds. They mentioned that the river beds follow relatively weak fractured zones. Thus mapping the river course using satellite radar provided location estimates of relatively highly fractured zones.

Azimuthal Velocity Anisotropy: Velocity anisotropy in the present context refers to different acoustic (sound wave) velocity magnitudes in different horizontal directions. This phenomenon aids in detecting subsurface fractures and their general orientation. It is commonly determined using a borehole dipole sonic tool that consists of mutually perpendicular pairs of dipole transmitters and receivers. In isotropic formations, both receivers measure the similar shear wave arrival times. In anisotropic formations, however, the arrival times are different. A difference in fast and slow shear-wave velocities (i.e., different arrival times) is an indicator of the magnitude of anisotropy [50] due to joints, faults, inclined bedding planes, and tectonic stresses. Fast shear-wave azimuth generally indicates the direction of maximum horizontal stress. However, given a vertical well, nearly horizontal bedding, and isotropic state of stress (i.e., minimum and maximum horizontal stresses are nearly equal), the azimuth of the fast shear wave is interpreted as being parallel to the general direction of fracture strikes. In addition to the borehole, fast and slow velocity anisotropy can also be observed using seismic data [51-53].

Miscellaneous Indirect Joint Characterization Methods: Additional indirect methods of ascertaining fracture presence and connectivity in the subsurface include distributed temperature sensors, crosswell salinity measurements, and crosshole pressure measurements [48]. Hoffman and Narr [54] demonstrated the use of production logging data along with borehole image logs and simulation models to estimate the natural fracture sizes with the ultimate aim of understanding fracture interconnectivity and reservoir drainage patterns. Quinn, et al. [55] used straddle packer tests, which include constant head step tests, slug tests, pumping tests, and recovery tests to help ascertain fracture hydraulic apertures.

This section does not present an exhaustive list of auxiliary methods of indirect joint characterization. Other tools may exist already or currently under development.

Discussion and Recommendation

Careful scrutiny is required while determining joint origin timing. For example, joint sets oriented nearly 60° apart should not inevitably be interpreted as shear fractures. In such cases, fracture faces should be scrutinized in order to ascertain signs of shear. The absence of such signs, or the selective occurrence of such conjugate-looking joints in adjacent beds of markedly different lithologies, may indicate separate origins. Also, joints oriented parallel or perpendicular to the fold axis should not automatically be interpreted as fold related. In other words, prefolding factures may be mistakenly interpreted as fold related since they will predictably be present across the fold in some orientation. Crosscutting, termination, cementation (bitumen, quartz, calcite etc.), graphical bed restoration (unfolding), and prior knowledge of tectonic regimes must be utilized in such instances to differentiate fold-related joints from prefolding ones. Similarly, careful scrutiny is required for assigning origin timings and driving factors behind non-fold-related (prefolding) joints.

We mentioned several direct and indirect joint characterization data sources. While outcrops, image logs, and cores provide direct joint observations, geophysical, chemical, and engineering methods are semi quantitative to qualitative (i.e., infer the presence and relative abundance of natural fractures). A major benefit of the indirect methods such as microseismic, GPR, straddle

packer tests, and crosswell salinity tests is their ability to provide in-situ reservoir information. A limitation, however, is that these measurements require substantial capital investment. Methods such as wellbore velocity anisotropy require dipole sonic logs (which are often not acquired) to ascertain the presence and orientation of natural fractures near the wellbore. Semi-quantitative fracture abundance determination (through neural network models) in the entire reservoir volume of interest requires seismic data requiring tens of millions of Dollars in investment. Direct measurements from outcrops and well logs overcome some of these limitations presented by the aforementioned indirect data sources of fracture characterization.

Considering direct fracture observation methods, obtaining core and image logs also require substantial capital expenditure. Additionally, observations derived from cores and logs only present limited information on joint abundance and geometry due to truncation beyond the borehole/core volume. Outcrops, on the other hand, can provide a range of joint abundance and geometry parameters, i.e., height, aperture, length, cementation, lateral and vertical abundance, bed-boundedness, and termination/crosscutting relationships. Length-height relationships and length-aperture relationships of long fractures, which are the main fluid carriers, can only be obtained through outcrops. Moreover, the amount of information on joint origin timing and stress history that can be obtained from outcrops is virtually impossible from any aforementioned single direct or indirect source of joint data. Therefore, upon availability, outcrops must be included in joint related studies.

However, the fact that outcrops provide such a wide variety of information, comes with a caveat. Joints observed at outcrops may result from stress release, weathering, roadside blasting (near road cuts), and quarrying activities, obscuring the relevant subsurface joint related information. Therefore, it is necessary to differentiate and filter out fractures that only exist at outcrops and not the nearby shallow or deep subsurface. Therefore, comparison of multiple outcrop fracture parameters to multiple core and log data from adjoining areas may provide greater confidence in outcrop joint interpretations.

Several direct joint abundance characterization methods were also discussed. The appropriate characterization method for a given scenario depends on the data source and the data requirement. In cores, the number of joints (P10) in a unit length of slab/butt planar face, total number of joints in a unit area (P20) of slab/butt planar face, and total length of joints in a unit area (P21) of slab/butt planar face, along the core length are few ways of characterizing abundance. Cumulative apertures may be plotted along several short scanlines oriented perpendicular to the joints to find several values of linear porosity (P11). Joint aperture and height (if the full trace is visible) distribution may be taken from joints in a given slab/butt planar face area or along a scanline. However, 2-4 inches (5.1-10.2 cm) of scanline (oriented perpendicular to the core length) may be too short for obtaining reasonable values. Characterization from image logs is similar to that from the cores.

If an outcrop stratigraphic section is available, bed by bed joint intensity (P10) along scanline lengths may be useful for characterizing fracture abundance along the stratigraphic section. Additionally, P21, P20, and P11 measurements may be obtained in a manner similar to that described for the core, albeit on much larger surface areas. The P21 method may be especially suitable for tall fractures. Joint height distribution, i.e., the statistical distribution of vertical traces along a scanline or in a chosen cliff face area may be measured as well. On the other hand, if only a few horizontal bedding surfaces are visible (as in a map view) in a large area, both P10, P11 (along scanlines) and P21 (in a given area) may be measurable. Also, the joint length distributions (i.e., statistical distribution of horizontal traces) along a scanline may be obtained if complete trace lengths are visible. Additionally, the joint length statistical distributions in a given area (observed in a map view) may also be obtained.

Additionally, joint aperture vs. height correlation may also be determined in a cliff face (i.e., bed cross-section) view and joint length vs. aperture correlation may be determined in a bed face view (i.e., map view). However, in both cases, a representative aperture value may be required for each joint due to spatial variation in the joint aperture. Moreover, if several joints are exposed in their entirety in a cliff-face view, joint length vs. height correlations may be obtained.

References

1. Aydin A (2014) Failure modes of shales and their implications for natural and manmade fracture assemblages. AAPG Bulletin 98(11): 2391-2409.

2. Pollard D, Aydin A (1988) Progress in understanding jointing over the past century: Geological Society of America Bulletin 100(8): 1181-1204.

3. Stearns DW, Friedman M (1972) Reservoirs in fractured rock: King RE (Ed.), AAPG Memoir Stratigraphic Oil and Gas Fields-Classification, Exploration Methods, and Case Histories. American Association of Petroleum Geologists and Society of Exploration Geophysicists 16: 82-106.

4. Bergbauer S, Pollard DD (2004) A new conceptual fold-fracture model including prefolding joints, based on the Emigrant Gap Anticline. Wyoming. GSA Bulletin 116(3-4): 294-307.

5. Cosgrove JW (2001) Hydraulic fracturing during the formation and deformation of a basin: a factor in the dewatering of low-permeability sediments. AAPG Bulletin 85(4): 737-748.

6. Lash GG, Engelder T (2005) An analysis of horizontal microcracking during catagenesis: Example from the Catskill delta complex: AAPG Bulletin 89(11): 1433-1449.

7. Ghosh S, Galvis Portilla HA, Klockow CM, Slatt RM (2018) An application of outcrop analogues to understanding the origin and abundance of natural fractures in the Woodford Shale. Journal of Petroleum Science and Engineering 164: 623-639.

8. Pireh A, Alavi SA, Ghassemi MR, Shaban A (2015) Analysis of natural fractures and effect of deformation intensity on fracture density in Garau formation for shale gas development within two anticlines of Zagros fold and thrust belt, Iran. Journal of Petroleum Science and Engineering 125: 162-180.

9. Hooker JN, Laubach SE, Marrett R (2013) Fracture-aperture size-Frequency, spatial distribution, and growth processes in strata-bounded and nonstrata-bounded fractures, Cambrian Mesón Group, NW Argentina. Journal of Structural Geology 54: 54-71.

10. Mauldon M, Dershowitz B (2000) A multi-dimensional system of fracture abundance measures. Geological Society of America Annual Meeting, Nevada, pp: 1-28.

11. Zeeb C, Gomez-Rivas E, Bons PD, Blum P (2013) Evaluation of sampling methods for fracture network characterization using outcrops. AAPG Bulletin 97(9): 1545-1566.

12. Ghosh S (2017) Integrated studies on Woodford Shale natural fracture attributes, origin, and their relation to hydraulic fracturing. Ph.D. Dissertation, University of Oklahoma, Norman, OK.

13. Barthelemy JF, Guiton MLE, Daniel JM (2009) Estimates of fracture density and uncertainties from well data. International Journal of Rock Mechanics and Mining Sciences 46(3): 590-603.

14. Priest SD (1993) Discontinuity analysis for rock engineering: 1st (Edn.), London, United Kingdom, Chapman & Hall.

15. Ghosh S (2017) Multiscale Natural Fracture Dimensions in the Woodford Shale. Search and Discovery Article #51405. AAPG Southwest Section Meeting, Midland, Texas, pp: 1-18.

16. Olson JE (2003) Sub linear scaling of fracture aperture versus length: An exception or the rule? Journal of Geophysical Research 108(B9): 2413.

17. Ghosh S, Bontempi CP, Hooker JN, Slatt RM (2018) High-resolution stratigraphic characterization of natural fracture attributes in the Woodford Shale, Arbuckle Wilderness and US-77D Outcrops, Murray County, Oklahoma. Interpretation 6(1): SC29-SC41.

18. Hanzel J (2012) Lidar-based fracture characterization: an outcrop-scale study of the Woodford Shale, McAlister Shale Pit, Oklahoma. M.S. Thesis, Oklahoma State University, Stillwater, OK.

19. Schlichtemeier B (2011) LIDAR characterization and reservoir modelling of an Upper Jack fork Group basin floor fan deposit at Degray Spillway, Caddo Valley, Arkansas. M.S. Thesis, University of Oklahoma, Norman, OK.

20. Portas RA (2009) Characterization and origin of fracture patterns in the Woodford Shale in Southeastern Oklahoma for application to exploration and development. AAPG Annual Convention and Exhibition, New Orleans, Louisiana.

21. Ahmedhadi F, Lacombe O, Daniel JM (2007) Early reactivation of basement faults in Central Zagros (SW Iran): Evidence from pre-folding fracture populations in the Asmari Formation and Lower Tertiary paleogeography. In: Lacombe O, Roure F, Lave J, Verges J (Eds.), Thrust Belts and Foreland Basins. Springer, Berlin, Heidelberg, pp: 205-228.

22. Hilgers C, Kirschner DL, Breton JP, Urai JL (2006) Fracture sealing and fluid overpressures in

limestones of the Jabal Akhdar dome, Oman Mountains. Geofluids 6: 168-184.

23. Holland M, Saxena N, UraiJ L (2009) Evolution of fractures in a highly dynamic thermal hydraulic, and mechanical system-(II) Remote sensing fracture analysis, Jabal Shams, Oman Mountains GeoArabia 14(3): 163-194.

24. Holland M, UraiJ L, Muchez P, Willemse EJM (2009) Evolution of fractures in a highly dynamic, thermal, hydraulic, and mechanical system-(I) Field observations in Mesozoic carbonates, Jabal Shams, Oman Mountains. Geo Arabia 14(1): 57-110.

25. Zeeb C, Gockus D, Bons PD, Ajmi HA, Rausch R, et al. (2010) Fracture flow modelling based on satellite images of the Wajid Sandstone, Saudi Arabia. Hydrogeology Journal 18(7): 1699-1712.

26. Dinger JS, Andrews RE, Wunsch DR, Dunno GA (2002) Remote sensing and field techniques to locate fracture zones for high-yield water wells in the Appalachian Plateau, Kentucky. Proceedings of the National Ground Water Association Fractured-Rock Aquifer Conference, March 13-15, Denver, Colorado.

27. Geo Vision, geophysical method.

28. Milad B, Ghosh S, Suliman M, Slatt RM (2018) Upscaled DFN models to understand the effects of natural fracture properties on fluid flow in the Hunton Group tight Limestone. Unconventional Resources Technology Conference, Houston, Texas, USA.

29. Terzaghi RD (1965) Sources of error in joint surveys: Geotechnique 15(3): 287-304.

30. Milad B, Ghosh S, Slatt RM (2018) Comparison of rock and natural fracture attributes in karsted and non-karsted Hunton Group Limestone: Ada and Fittstown area, Oklahoma. The Shale Shaker 69(2): 70-86.

31. Gale JFW, Laubach SE, Olson JE, Eichhubl P, Fall A (2014) Natural fractures in shale: A review and new observations. AAPG Bulletin 98(11): 2165-2216.

32. Fisher MK, Wright CA, Davidson BM, Goodwin AK, Fielder EO, et al. (2005) Integrating fracture-mapping technologies to improve stimulations in the Barnett Shale. SPE Production and Facilities 20(2): 85-93.

33. Dunphy R, Campagna DJ (2011) Fractures, elastic moduli & stress: Geological controls on hydraulic fracture geometry in the Horn River Basin. Recovery, 2011 CSPG CSEG CWLS Convention, pp: 1-9.

34. Fisher MK., Warpinski NR (2012) Hydraulic-fracture-height growth: Real data. SPE Production & Operations 27(1): 8-9.

35. Backus GE, Gilbert F (1970) Uniqueness in the inversion of inaccurate gross Earth data. Philos Trans Roy Soc A 266(1173): 169-205.

36. Stump BW, Johnson LR (1977) The determination of source properties by the linear inversion of seismograms. Bull Seism Soc Am 67(6): 1489-1502.

37. Urbancic TI, Trifu CI, Young RP (1993) Microseismicity derived fault-planes and their relationship to focal mechanism, stress inversion, and geologic data. Geophys Res Lett 20(22): 2475-2478.

38. Baig AM, Urbancic T (2010) Microseismic moment tensors: A path to understanding frac growth. The Leading Edge 29(3): 320-324.

39. Bosman K, Urbancic T, Ardakani EP (2018) Characterizing Microseismic-Derived Fracture Networks in the Context of Connectivity and Fluid Flow. American Rock Mechanics Conference, Seattle, Washington, 20-22.

40. Zellou AM, Ouenes A, Banik AK (1995) Improved Fractured Reservoir Characterization Using Neural Networks, Geomechanics and 3-D Seismic. SPE Annual Technical Conference Dallas, TX, USA, pp: 22-25.

41. Jenkins C, Ouenes A, Zellou A (2009) Quantifying and predicting naturally fractured reservoir behavior with continuous fracture models. AAPG Bulletin 93(11): 1597-1608.

42. Beres M, Green A, Huggenberger P, Horstmeyer H (1995) Mapping the architecture of glaciofluvial sediments with three-dimensional georadar. Geology 23(12): 1087-1090.

43. Bridge JS, Alexander J, Collier RE, Gawthorpe RL, Jarvis J (1995) Ground-penetrating radar and coring used to study the large-scale structure of point-bar deposits in three dimensions: Sedimentology 42(6): 839-852.

44. Dominic DF, Egan K, Carney C, Wolfe PJ, Boardman MR (1995) Delineation of shallow stratigraphy using

ground-penetrating radar. Journal of Applied Geophysics 33(1-3): 167-175.

45. Martinez A, Kruger JM, Franseen EK (1998) Utility of Ground-penetrating Radar in Near-surface, High-resolution Imaging of Lansing-Kansas City (Pennsylvanian) Limestone Reservoir Analogs. Utility of Ground-penetrating Radar in Imaging of Limestone Reservoir Analogs, pp: 44-59.

46. Pratt BR, Miall AD (1993) Anatomy of a bioclastic grainstone megashoal (Middle Silurian, southern Ontario) revealed by ground-penetrating radar. Geology 21(3): 223-226.

47. Liner CL, Liner JL (1995) Ground penetrating radar-A near-face experience from Washington County, Arkansas: The Leading Edge 14(1): 17-21.

48. Jalali MR, Klepikova M, Doetsch J, Krietsch H, Brixel B (2018) A Multi-Scale Approach to Identify and Characterize Preferential Flow Paths in a Fractured Crystalline Rock. American Rock Mechanics Association (ARMA).

49. Laake A (2011) Integration of Satellite Imagery, Geology and Geophysical Data. IntechOpen, pp: 467-492.

50. Sinha BK, Kane MR, Frignet B (2000) Dipole dispersion crossover and sonic logs in a limestone reservoir. Geophysics, 65(2): 390-407.

51. Takanashi M, Tsvankin I (2012) Moveout inversion of wide-azimuth data in the presence of laterally varying velocity. Geophysics 77(3): U49-U62.

52. Al-Chalabi M (1979) Velocity determination from seismic reflection data. In: Fitch AA (Ed.), Developments in Geophysical Exploration Methods-1. Springer, Dordrecht, pp: 1-68.

53. Biondi B (2006) 3D Seismic Imaging. Society of Exploration Geophysicists, pp: 247.

54. Hoffman BT, Narr W (2012) Using production logs (PLT) to estimate the size of fracture networks. Journal of Petroleum Science and Engineering 98-99: 11-18.

55. Quinn P, Cherry J, Parker B (2013) The use of straddle packer testing to hydraulically characterize rock boreholes for contaminant transport studies. Presentation for the Solinst Symposium, pp: 1-85.